Available online at www.sciencedirect.com

ScienceDirect

Advances in Space Research 55 (2015) 2058–2069

ADVANCES IN SPACE RESEARCH (a COSPAR publication)

www.elsevier.com/locate/asr

Ionospheric specification with analytical profilers: Evidences of non-Chapman electron density distribution in the upper ionosphere

T. Verhulst *, S.M. Stankov

Royal Meteorological Institute (RMI), Ringlaan 3, B-1180 Brussels, Belgium

Received 24 March 2014; received in revised form 8 October 2014; accepted 16 October 2014
Available online 23 October 2014

Abstract

In relation to the development of an operational ionospheric monitoring and imaging system, the most frequently used analytical ionospheric profilers (Chapman, Epstein, Exponential) were investigated in terms of suitability for topside ionosphere modelling. For the purpose, topside sounder measurements onboard Alouette and ISIS satellites have been analysed. We have come to the conclusion that the use of the Chapman profiler should be exercised with precaution as there are evidences that there are conditions when other profilers are better fit for modelling purposes. This is highlighted during ionospheric disturbances (e.g. during geomagnetic storms), when the shape of the topside electron density distribution might be better described by an Epstein profiler rather than a Chapman profiler.

Keywords: Ionospheric profiler; Total electron content; Slab thickness; Geomagnetic storm

1. Introduction

Ionospheric modelling is essential in the overall space weather monitoring and mitigation of the related influences. Modelling the topside ionosphere, the region above the height (h_mF_2) of the peak of ionosphere density (N_mF_2), poses particular difficulties. While the bottomside ionosphere is easily accessible for ground-based observation, e.g. by the traditionally-used vertical incidence sounder (ionosonde), such ionosonde measurements alone are not able to deliver information about the topside ionosphere and thus to provide data for empirical modelling. There are other means (rather expensive) to collect such information, mostly via rocket and satellite in-situ measurements, coherent and incoherent scatter radar probing, topside sounding using ionosondes onboard satellites, and more recently, the ionospheric radio occultations.

Over the years, theoretical modelling efforts led to the development of various ionospheric models, from relatively simple ones to complex, global multi-dimensional models. Some of the most frequently used simple models of the vertical electron density distribution are the Exponential, Chapman and Epstein profile models, also called profilers (Appendix A). Of them, the Chapman profiler is particularly popular (e.g. Reinisch and Huang, 2001; Bilitza, 2004; Feltens, 2007; Tulasi Ram et al., 2009). A nice feature of the Chapman profiler is that it needs only the ionospheric peak density (N_mF_2), peak height (h_mF_2), and an estimate of the scale height to calculate the distribution (profile) of electron density in the topside ionosphere. However, since the constructed profile is not tied to any additional measurements, its (indiscriminate) use is vulnerable to over-simplification of the plasma distribution, especially in a region known for its dynamic nature. One proposed improvement is to use a combination of multiple profiles, with different scale heights (Fonda et al., 2005; Kutiev et al., 2006a), or with scale heights varying with height (Reinisch et al., 2007; Nsumei et al., 2012).

* Corresponding author. Tel.: +32 (0)60/395472; fax: +32 (0)60/395423.
E-mail addresses: tobias.verhulst@meteo.be (T. Verhulst), s.stankov@meteo.be (S.M. Stankov).

http://dx.doi.org/10.1016/j.asr.2014.10.017
0273-1177/

However, these more sophisticated models still rely on the assumption that the shape of the topside profile is essentially a Chapman curve.

An operational local ionosphere monitoring system, based on ionosonde and GNSS measurements for deducing and imaging the vertical distribution of electron density, has been developed and installed at the RMI Geophysical Centre in Dourbes (50.1N, 4.6E) (Stankov et al., 2011, more details in Appendix B). As part of the evaluation process and further improving the system, we used topside sounder measurements (onboard Alouette and ISIS satellites) to find out which of the abovementioned profilers yield better results and under what circumstances (Verhulst and Stankov, 2013; 2014). The electron density profiles measured by the topside sounders have been fitted with each of the theoretical ionospheric profilers and the corresponding approximation errors were calculated. The approximation results were analysed with respect to "external" factors (local time, geomagnetic latitude, season, and solar activity), as well as to the key characteristics of the topside ionosphere (N_mF_2, h_mF_2, and the upper transition level, UTL). One important finding is that, although there is an influence of these external factors on the shape of the density profile, the indices representing these factors (such as K_p or Dst) are unsuitable for selecting the "best" profile. Better selection criteria are offered by the key ionospheric characteristics, a possible explanation being that these characteristics react to the external factors thus intrinsically contain the necessary information for the selection process.

The aim of the here-presented study is to provide evidences of the diversity of plasma distribution (non-Chapman in particular) in the upper ionosphere and to analyse the conditions leading to this variety. In doing so, additional key ionospheric characteristics, such as the total electron content (TEC) and ionospheric slab thickness, are utilised.

The paper outline is as follows. First, the measurements used for this work are presented. The next section provides some evidences of profiles best fitted by non-Chapman profilers. This is followed by analysis of the TEC and slab thickness relations to the shape of the topside electron density profile (EDP). After that, we focus on the ionospheric storm-time behaviour of the TEC and slab thickness. The paper concludes with a discussion of the results in view of the possibilities they offer for improving the profiler selection for the LIEDR (Local Ionospheric Electron Density profile Reconstruction) procedure.

2. Data

2.1. Space-based measurements (topside sounders)

For this work, we use the data from the topside ionosondes that flew on the Alouette-1 and -2 and ISIS-1 and -2 satellites (Jackson, 1969; Jackson and Warren, 1969; Jackson et al., 1980; Jackson, 1988). These data are available from NASA/GSFC's Space Physics Data Facility (SPDF) and include electron density profiles that had been obtained from manually scaled ionograms in the 1970s (Bilitza et al., 2003) and more recently with the Topside Ionogram Scaler With True Height Algorithm (TOPIST) software (Bilitza et al., 2004; Benson, 2010). This collection contains more than 170,000 electron density profiles. The first of the four satellites, Alouette 1, started its soundings in 1962, while the final measurements in this dataset (ISIS-1) date back to 1981. Data is therefore available covering more than one complete solar cycle. Unfortunately, the data distribution, both temporal and spatial, is very irregular which gives rise to systematic biases and data selection problems that have to be corrected for (Verhulst and Stankov, 2013; 2014). Also, not all available profiles are useful for our study, because we can only use those that cover the entire region between the F_2 peak and the upper transition height (Verhulst and Stankov, 2013).

For the purpose of this study, it is important that the data also cover all magnetic conditions. From Table 1 it can be seen that 7.88% of the profiles were measured when Dst was below -50, an indication of a geomagnetic storm; or 6.15% when $K_p \geqslant 5$, if the K index is used to indicate storm conditions. Additionally, 25.28% of the measurements were taken when the K index was 3 or 4, signifying minor geomagnetic disturbances. This gives an opportunity to study the influences on the topside shape during disturbances of different severity (Warren, 1969).

2.2. Ground-based measurements (ionosonde and GNSS)

For many years, the Dourbes ionosonde (URSI code: DB049) has been carrying out regular vertical ionospheric soundings with Lowell digital ionospheric sounders, previously DGS-128, DGS-256, and since April 2011, Digisonde-4D® (Reinisch et al., 2009). All ionograms are automatically scaled and the values of f_oF_2, f_oE, $M_{3000}F_2$, and h_mF_2 are deduced with only a short delay. Some of the current ionosonde settings are: frequency range 1.0–16.0 MHz (daytime) and 0.5–12.0 MHz (nighttime), frequency scale – linear, coarse frequency step – 25 kHz, fine frequency step – 5 kHz, range 80–1500 km, range resolution – 2.5 km, integrated repeats – 4, ionogram duration – 150 s. Currently, the sounding rate (cadence) is set to one every 5 min, but it can be further increased if necessary. The automatic scaling of ionograms has been evaluated (Stankov et al., 2012) and error bounds have been

Table 1
Availability of topside sounder measurements under different geomagnetic activity conditions as represented by the K_p (left) and Dst (right) indices.

K_p index	Dst index		
0–2	68.57%	$\geqslant 0$	29.93%
3	16.28%	−50 to 0	62.19%
4	9.00%	−100 to −50	6.34%
$\geqslant 5$	6.15%	<-100	1.54%

determined (95% probability) for the following characteristics: f_oF_2 (−0.75,+0.85 MHz), f_oE (−0.35,+0.40 MHz), $h'F_2$ (−68,+67 km), $h'E$ (−26,+2 km), and $M_{3000}F_2$ (−0.55,+0.45).

Local TEC observations have been made with a GPS receiver applying a computational procedure based on the 'geometry-free' combination of GPS code and phase measurements for fixing the ambiguities. Receiver and satellite group delays were estimated by modelling the slant TEC with a polynomial depending on latitude and local time. The conversion to vertical TEC was performed by assuming the standard ionospheric thin-shell model at a mean ionospheric height of 350 km. The TEC data base consists of measurements since 1994, i.e. covering more than one complete solar cycle period (Stankov et al., 2011, and references therein). Vertical TEC data, retrieved from the global ionosphere maps (Hernandez-Pajares et al., 2009), were also utilised as an additional reference and for deducing the latitudinal dependence of the storm-time variations.

3. Non-Chapman distribution – evidences deduced from topside sounder measurements

For a long time, the Chapman profiler has been widely used in ionospheric modelling of the topside ionospheric electron density. However, topside sounder measurements provide evidences that the topside electron density distribution may not necessarily follow such "Chapman" specification, and instead be better modelled by other profilers. A recent study (Verhulst and Stankov, 2014) revealed that, not only the measured profiles are better fitted by different analytical shapes but, also, it is necessary to use different scale heights for the different profile shapes. Moreover, correlations have been established between various intrinsic ionospheric characteristics (N_mF_2, h_mF_2,...) and external factors (local time, magnetic coordinates, season,...).

The area enclosed between the measured profile and the fit, from the peak height up to the transition height, was used as a measure of fit quality. Deviations occurring above the transition height have less weight in the fitting procedure—the focus really is on delivering best quality fit in the lower part of the topside ionosphere. This is done because, on the one hand, the different profilers are designed mainly for this region, and, on the other hand, this is the part with much higher electron density, thus contributing the most to the abovementioned measure of fit.

Some representative examples of measurements, obtained at various spatial and geophysical conditions and best fitted by either the α-Chapman or the Epstein profiler, are shown in Fig. 1. However, the two curves in each panel show topside electron densities for similar local times, and for the same season. The solar activity is also similar, except for the summer time plots. The local time effects can be clearly seen when comparing the peak densities of the left and right panels.

The observed differences between the two shapes are most likely the result of the magnetic conditions at the time of the measurements, or – in the case of post-storm depletions – the magnetic condition during the previous days. For example, the profiles obtained during equinox night time were measured when D_{st} was −106 (for the Epstein profile) and −19 (for the α-Chapman profile). For the summer, night-time profiles, the one measured during storm time (with $D_{st} = -51$) even crosses the one measured under quiet conditions ($D_{st} = -2$). This shows clearly that not only was the peak density diminished during the storm, but the shape of the profile was also different: a uniform depletion at all altitudes would result in profiles that never cross each other. To some extent, the same effect can be seen in all six panels.

4. Relation of the topside profile with topside TEC and slab thickness

As mentioned in the introduction, a previous study revealed that a more reliable selection of a profiler comes from the ionospheric density peak characteristics (N_mF_2 and h_mF_2). Here we will try to find further clues that other profile characteristics, such as the slab thickness and TEC, may provide. In Fig. 2A, it can be seen that the majority of profiles are best fitted with an α-Chapman profiler, but for a significant minority the Epstein curve gives better results. It is also clear from this figure that the most common topside TEC values, in general, are between 4 TECu and 9 TECu but that profiles best fitted by the Epstein profiler are most likely to have a TEC below 4 TECu. Fig. 2B shows the percentage of profilers best fitted by either the Epstein or the α-Chapman profiler, as a function of topside TEC. For TEC larger than 6 TECu, more than 90% of the profiles have an α-Chapman shape. For smaller TEC values this percentage drops quickly, down to between 60% and 70% for 2 TECu or lower. Notice that (cf. Fig. 2A) there are only a few cases of TEC being below 0.5 TECu, so the extreme, leftmost values in Fig. 2B might be due to insufficient data). These small values of TEC occur mostly during the nights after a geomagnetic storm (Buonsanto, 1999). Thus, in the aftermath of a storm, it is more likely that the topside profile follows an Epstein curve. It should be noted, however, that at all topside TEC values there are profiles with an α-Chapman shape. This is to be expected, since the data was taken at all possible local times and seasons and at different magnetic longitudes and latitudes; it is well known that the storm time behaviour at different times and location can be very different (Ondoh, 1967; Sato, 1968; Warren, 1969; Fuller-Rowell et al., 1994; Kutiev and Muhtarov, 2001), and it should be noted that a TEC value that is considered depleted at certain times and locations might be a normal, quiet time value at others (Kutiev et al., 2005; 2006b). The same issues exist with regard to the topside slab thickness (defined as the topside TEC divided by the peak electron density), which are displayed in Fig. 2C and Fig. 2D. These results

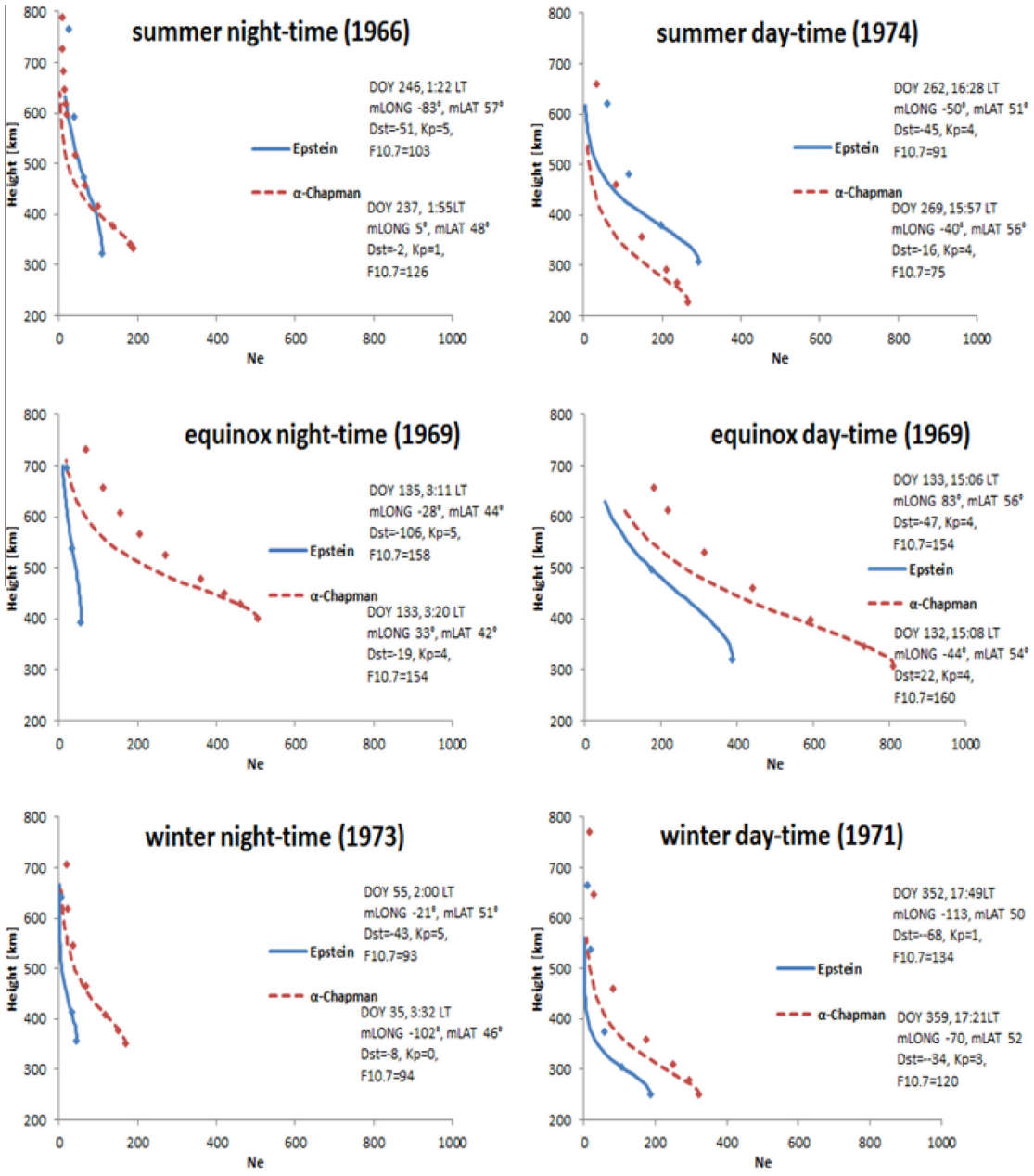

Fig. 1. Electron density profiles, as obtained from topside sounder measurements (denoted with symbols, rombs) and fitted with α-Chapman (dashed line, red) or Epstein (solid line, blue) profilers. The panels on the left side show the results for local night-time measurements and on the right side – for day-time measurements. The panels on the top show cases in summer, the ones in the middle – at equinoxes, and at the bottom – in winter. Further details on the measurements (coordinates, day of year, local time, solar and magnetic activity indices) are provided inside each plot. (For interpretation of the references to colour in this figure legend, the reader is referred to the web version of this article.)

might be greatly improved when, in the future, new topside sounders provide enough data to calculate reliable mean values, so as to be able to study relative topside TEC and topside slab thickness instead of absolute values.

Verhulst and Stankov (2014) have already pointed out that different ionospheric characteristics – N_mF_2, h_mF_2, scale height, distance from the F_2 -peak to the UTL, and others - are related to the shape of the topside electron density distribution, but that no single parameter can be used as a deciding factor in choosing an appropriate topside profiler. Thus, when modelling the topside profile, the TEC has to be used in combination with one or more other characteristics in order to select the best profiler.

5. Storm-time behaviour of TEC and slab thickness

For the purpose of this study we considered all geomagnetic storms that occurred between January 1994 and December 2009, i.e. during the entire solar cycle 23 (Stankov et al., 2010). The main reference used for selecting and analysing the geomagnetic storms was the D_{st} index. The selected storms were classified according to their

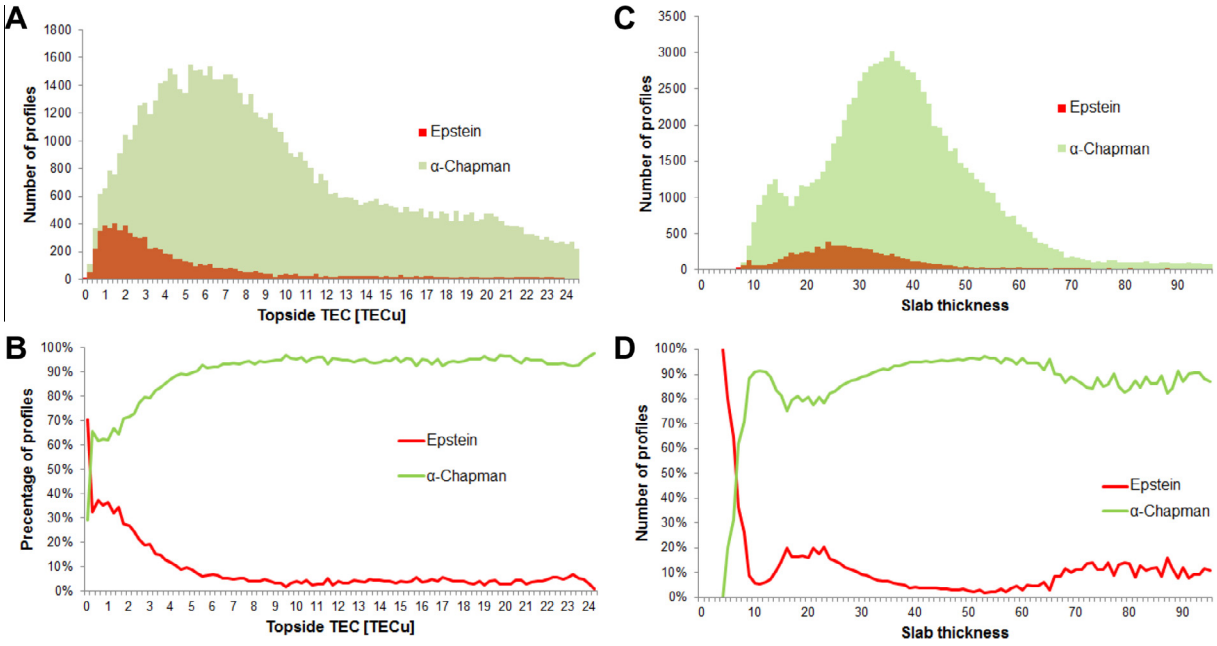

Fig. 2. Number of used Epstein and α-Chapman profiles relative to the topside TEC value (left panels) and topside slab thickness (right panels): total number (top panels) and percentage ratio (bottom panels).

intensity as Class I ($Dst_{min} \leqslant -100$nT) and Class II (-100nT $< Dst_{min} \leqslant -50$nT). TEC data representing nearly 300 storm events have been analysed with respect to geomagnetic storm intensity, season, latitude, and local time of the storm onset. When analysing TEC variations during geomagnetic storms, it is preferable to use the relative deviation (TEC_{rel}) of the observed TEC (TEC_{obs}) from normal (non-disturbed) conditions (in this study, the 27-day running median, TEC_{med}, for each hour of the day):

$$TEC_{rel} = \frac{TEC_{obs} - TEC_{med}}{TEC_{med}}. \quad (1)$$

To correctly deduce the average storm-time changes in the TEC_{rel} behaviour, a superposed epoch analysis (D_{st} and TEC measurements arranged according to the storm onset, ST = 0) was carried out for all storm periods.

The results of the epoch analysis using hourly medians (with reference to each storm time hour) of D_{st} and TEC_{rel} are shown here (Fig. 3) for equinox Class-I storms for the Dourbes station. The vertical axis corresponds to the D_{st} index (solid curve) and the relative percentage of TEC (vertical bars). The horizontal axis is the storm time (in hours), ranging from -24ST (i.e. 24 h before the start) through +120ST (i.e. 120 h after the start). Results for storm onsets during day are shown on the top, for those during night – at the bottom.

It is known that ionospheric response to geomagnetic forcing depends on local time (e.g. Proelss, 1984). For storms starting during daytime, results show that, with reference to storm time, the TEC relative deviation increases during the onset and peaks a few hours into the main phase. Immediately after that, TEC_{rel} decreases sharply to form a long-lasting depression for about 24 h before starting to increase during the recovery phase and reach values typical for non-disturbed conditions. Interestingly, the relative TEC decreases repeatedly in the following nights. Such behaviour, appearing outside the initial and main phases of geomagnetic storms, are reportedly observed at other longitudes as well, and can be explained with changes in the atmospheric circulation, resulting in upward and downward movements of the ionosphere.

When the storm onset occurs during local night time, the TEC relative deviation starts increasing early in the onset phase, peaking at around ST = 0, and then slowly decreasing during the main phase. The negative TEC_{rel} phase starts near the end of the storm's main phase (ST = 12) and reaches an absolute minimum at ST = 24. Immediately after that, the TEC_{rel} begins a "recovery" to almost pre-storm values, i.e. $TEC_{rel} = 0$, some 12 h later. Again, the relative TEC decreases repeatedly in the following couple of nights, although the minima are not so pronounced. Note that the minima occur always during the night, for both the daytime and nighttime storm onsets. At the end of the geomagnetic storm, TEC_{rel} becomes positive again, a phenomenon known as a "post-storm enhancement" (PSE). It is similar to the one observed in the Asian sector (Kutiev et al., 2005; 2006b) and is explained with the electro-magnetic drift effects of the convection electric field penetrating deep into the low/equatorial latitude ionosphere. Most of the PSE events appear to also depend on local time (late afternoon to early evening hours).

The results show that the TEC response to geomagnetic storms does indeed depend on local time. There are obvious similarities in the relative TEC behaviour irrespective of the time of the storm onset, for example

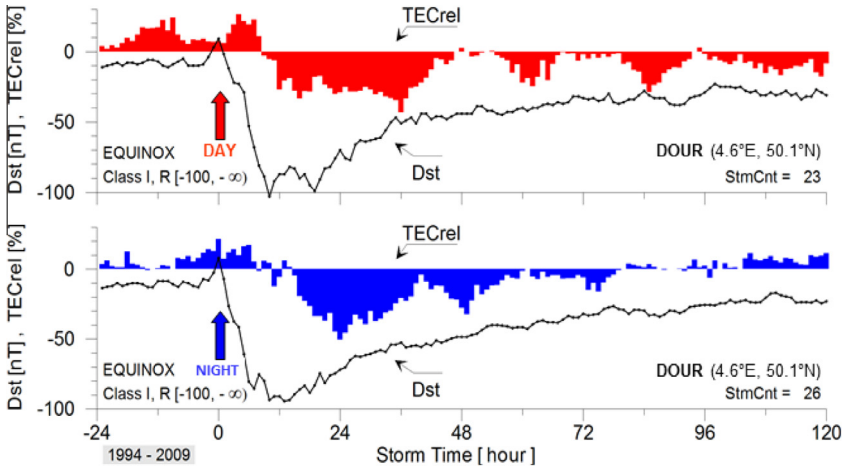

Fig. 3. Average GPS TEC relative deviations (TEC_{rel}) from 27-day medians during geomagnetic storms of class I during equinox, for storm onsets during day (top) and night (bottom) for the site of Dourbes (4.6° E, 50.1° N) based on data from 1994–2009.

the occurrence of a positive TEC phase around the onset and a negative phase characterised with several minima in the following nights. However, there are also substantial differences depending on the local time of the storm onset, most notably the timing of the positive phase maximum and the delayed negative phase during storms with night-time onsets. Such differences should be taken into account in ionosphere nowcast and forecast applications.

We have expanded the study to include another parameter, the ionospheric slab thickness (Appendix C). On average, active geomagnetic conditions tend to enhance the slab thickness (Fig. C1, Appendix C), more noticeably (in percentage terms) at high solar activity (HSA). Key factors affecting the storm-time perturbations of the slab thickness are the levels of the solar and geomagnetic activity, the season, and the storm onset time, among others.

Here we present the slab thickness perturbations during a recent geomagnetic storm in October 2013 (Fig. 4). Nominally, the geomagnetic storm started on 2 October 2013 at around 01:00 UT marked with the sharp increase in D_{st} up to a positive maximum at 02:00 UT before dropping rapidly to a minimum of y D_{st}=−75 nT at 07:00 UT in the same day. It was a Class II storm, lasting until the early hours of 6 October, which induced substantial response by the ionospheric characteristics f_oF_2, $h'F_2$, TEC, and the slab thickness. Around the start of the storm, both f_oF_2 and TEC enter a "positive" phase (absolute values above the medians) reaching a maximum of about 20% and 50% respectively. While the f_oF_2 positive phase ends a couple of hours into the main storm phase, the TEC maintains values above the median during the entire main phase and some hours at the beginning of the recovery phase. This results in a substantial increase of the relative slab thickness, reaching maximum values of almost 200% near the end of the main phase (Fig. 4A). After the main phase, both f_oF_2 and TEC enter into a negative phase (absolute values lower than the medians) and move

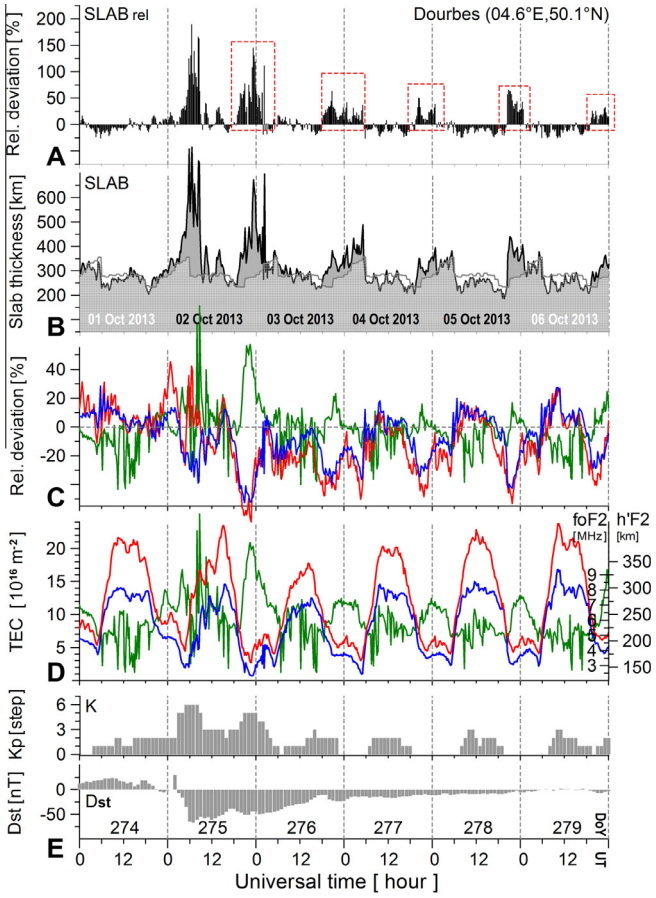

Fig. 4. Ionospheric and magnetic activity measurements at Dourbes, 01–07 October 2013. (A): Relative deviation (%) of the instantaneous ionospheric slab thickness from 27-day hourly medians (4–30 September 2014); (B): Instantaneous (black line) and median (grey line) slab thickness; (C): Relative deviations of TEC (red), f_oF_2 (blue), and $h'F_2$ (green); (D): Instantaneous measurements of TEC (red), f_oF_2 (blue), and $h'F_2$ (green); (E): Local magnetic K index (top) and geomagnetic storm-time index Dst (bottom). (For interpretation of the references to colour in this figure legend, the reader is referred to the web version of this article.)

"locked" together in phase for almost the entire recovery phase until 5 October (Fig. 4C). However, on several occasions (particularly during night) the negative phase of TEC is less pronounced than that of f_oF_2, i.e. $TEC_{rel} > F_oF_{2rel}$, which leads to positive slab thickness deviation in relative terms of up to 150% in the first night (2–3 October) following the storm onset (Fig. 4A). At the same time, the relative deviation of the peak height is clearly in anti-phase with the f_oF_2 and TEC deviations. During the following nights, the slab thickness exhibits a similar behaviour (albeit to a lesser extent) with values well above the medians (cf. the red rectangles in the top panel of Fig. 4). Such increases of the slab thickness during night, given the relatively low values of f_oF_2 and TEC, suggest steeper topside density profiles—a sign of plasma influx from above which "refills" the depleted ionosphere.

As discussed in section 4, there is a correlation between the (topside) TEC and the shape of the topside electron density profile. However, this need not, a priori, be the case. It is possible to contrive a distribution with enhanced or depleted TEC, yet maintaining the same qualitative shape. The topside slab thickness—the slab thickness calculated using only the topside TEC rather than the total TEC, as in Fig. 2C—can be interpreted as a measure for the steepness of the topside profile. When the slab thickness, too, is seen to deviate from its median values this does indicate a change in the shape of the distribution; either a change in the scale height or a change from a Chapman profile to an Epstein one. This should be carefully interpreted because changes in the total slab thickness, as shown in Fig. 4 and Fig. 5, are at least partially the result of changes in the bottomside region. However, because of the relation of topside profile shape with TEC and slab thickness, as seen in Fig. 2, it is to be expected that the topside electron distribution in such disturbed ionospheres deviates from the α-Chapman profile. In most cases analysed in detail, the Epstein profiler gave a better fit to the topside electron distribution (see Fig. 1 for some examples). Note that it is to be expected that in a disturbed ionosphere the topside electron distribution no longer follows the α-Chapman profile, since this profile is only expected to be correct when there is little movement of the plasma. This, however, does not necessarily mean the profile has to follow the Epstein shape, or any of the shapes we considered. It is possible that the true shape of the topside profile is not described by any static profiler, but requires a dynamical description.

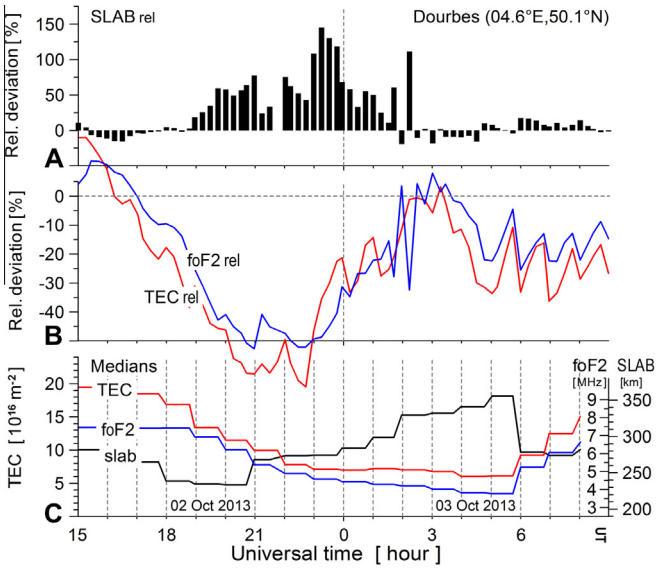

Fig. 5. Ionospheric and magnetic activity measurements at Dourbes, 2–3 October 2013. (A): Relative deviation (%) of the instantaneous ionospheric slab thickness from 27-day hourly medians (4–30 September 2014); (B): Relative deviations of TEC (red), and foF2 (blue); (C): Hourly medians of TEC (red), foF2 (blue), and slab thickness (solid black line). (For interpretation of the references to colour in this figure legend, the reader is referred to the web version of this article.)

6. Discussion

While there are physical arguments to expect the shape of the electron density profile in the topside ionosphere to resemble an α-Chapman curve, this is substantiated when the ionisation is locally produced, without major fluxes of ions. In the topside ionosphere and the plasmasphere the density of the neutral atmosphere components are so small that they have little effect on the charged particle motions (Banks and Kockarts, 1973; Davies, 1990). There is essentially no ion production; the ionisation is produced in the ionosphere during the day and diffuses upward. During night-time however, when the ionospheric plasma densities decrease, the plasma diffuses down (along the geomagnetic field lines) from the plasmasphere into the ionosphere. The presence of strong plasma flows is typical during the 'recovery' phase of the ionospheric storm when the upward flowing plasma fills the field tube along which the plasma moves towards diffusive equilibrium. The analytical models used here are known to describe typical diffusive equilibrium conditions.

The analysis of historical topside sounding data shows that there is a correlation between the shape of the topside electron density distribution and the total electron content: when the TEC value is low, the distribution is more likely to follow an Epstein curve rather than a Chapman profile. If the TEC value is large, the electron distribution is almost always better described by an α-Chapman profile. Correlations between this shape and other characteristics of the topside ionosphere—transition height, slab thickness, scale height—have already been established (Verhulst and Stankov, 2014).

Analysing the evolution of the TEC and slab thickness during a storm shows that, during the storm-time depletion of the ionosphere, the slab thickness typically increases together with the height of the F_2 peak. However, this increase in slab thickness is not necessarily due to high TEC values—the TEC values may be well below the average and still have relatively high slab thickness (cf. Fig. 5).

In such cases, the topside profile might be better described with an Epstein profiler.

A post-storm increase in TEC is also known (Kutiev et al., 2006b; Stankov et al., 2010). Considering the above analysis, in such situations apparently the Chapman profiler should be better suited for modelling purposes.

As already pointed out in Verhulst and Stankov (2014), neither the single characteristic of the ionosphere nor any of the usual indices for solar and magnetic activity can provide a firm basis for selecting the most appropriate topside profiler in all cases. The same holds true for the (topside) TEC, as was discussed in section 4. Therefore, we conclude that the most promising way to choose a profiler is to base this selection on multiple characteristics of the ionosphere. The most suitable characteristics seem to be the F_2 peak height and density, the slab thickness and the TEC (or topside TEC and bottom side TEC separately). In doing so, it has to be kept in mind that those characteristics are not mutually independent. The slab thickness is derived from the TEC and peak density, and therefore is, in essence, already a combination of two measured variables. The peak characteristics and topside (or bottomside) TEC are also not independent, as can clearly be seen from the example in Fig. 6. The red line in this figure shows a typical example for the electron density distribution during a geomagnetic storm: the ionosphere is depleted, with a significantly lower peak density but, at the same time, also a higher peak height. Even if the profile above this new peak is more or less unchanged, the topside TEC will still be a lot smaller than in quiet conditions.

The Chapman profiler is used in several well-known applications. The topside electron density model in the IRI is based on the Booker scheme (Booker, 1977) utilising the analytical model by Bent et al. (1972), which provides the exponential scale heights in three altitude regimes. In this model, the topside region is divided in 4 segments assuming a bi-parabolic variation in the lowest segment and exponential variation in the higher segments. In the development of the recent version of IRI, newly available topside sounder data was used to improve the topside profile representation (Bilitza, 2004). For this purpose, a Chapman layer is fitted (via a least-square fitting procedure) to the measured profiles to deduce the best Chapman parameters (peak height, density and scale height) to represent the topside ionosphere.

In Fig. 7 the number of topside profiles best fitted by the α-Chapman and Epstein profilers is shown in relation to the TEC calculated using the IRI model, which is included with the topside sounder data. It is clear that the result is very similar to Fig. 2A, which shows the relation with the TEC calculated from the measured profile—as is expected—albeit somewhat less pronounced. Since the IRI model produces the best results in quiet conditions, and the Epstein shaped profiles are associated with storms, it is understandable that the relation in Fig. 7 is less clear than in Fig. 2A, since precisely in the strongly disturbed, heavily depleted ionospheres deviations from IRI predictions can be expected. Nevertheless, it is still clear from Fig. 7 that the Epstein profiler is more usable at low TEC values. One possible future improvement of these results might come from using relative topside (and bottomside) TEC and slab thickness, instead of the absolute values discussed in section 4 and shown in Fig. 2. This, however, requires more data to be available in order to calculate mean values. This might be possible in the future using GNSS data or future topside ionosondes.

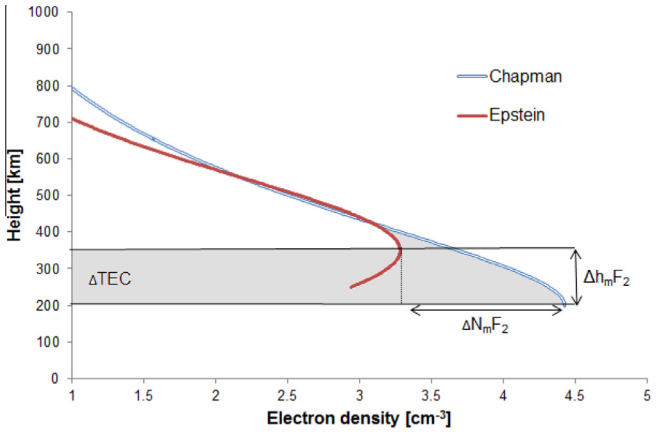

Fig. 6. An example of Chapman (blue) and Epstein (red) profiles, showing how in a depleted ionosphere the changes in peak height and density—$\Delta h_m F_2$ and $\Delta N_m F_2$—are related to each other and to the variation in (topside) TEC. (For interpretation of the references to colour in this figure legend, the reader is referred to the web version of this article.)

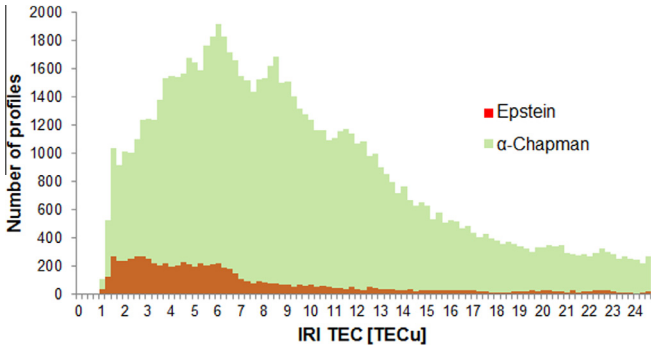

Fig. 7. Number of Epstein and α-Chapman profiles in relation to the topside TEC predicted by IRI (cp. Fig. 2).

Another application of the Chapman profile is in the topside profile construction offered by the Lowell Digisonde (Reinisch et al., 2009). In an earlier development, the topside electron density profile above the F2 layer peak was approximated by an α-Chapman function with a constant scale height that was derived from the bottomside profile shape near the F2 density peak (Reinisch and Huang, 2001). Later on, additional satellite-based information—from IMAGE/RPI measurements and ISIS topside sounders—was used to improve the topside profile representation (Reinisch et al., 2007; Nsumei et al., 2012) which is based again on an α-Chapman function, but with a varying scale height. These developments are also aimed at improving IRI.

7. Conclusion

This paper further investigates the use of simple analytical ionospheric profilers (Chapman, Epstein and Exponential) in terms of suitability for topside ionosphere modelling. Based on the Alouette and ISIS topside sounder database, an extensive statistical analysis has been performed to determine which of these profilers is best suited for ionospheric plasma density profile construction considering the varying geophysical condition in the local mid-latitude ionosphere. The particular focus here was on the use of the TEC and slab thickness to provide additional clues about the abovementioned profilers' suitability. The analysis shows that, in addition to N_mF_2 and h_mF_2, both the TEC and the slab thickness can be quite useful when developing criteria for selecting the profiler, especially during ionospheric disturbances associated with geomagnetic storms. For example, we found that when the TEC values are low, the topside electron density profile is best fitted with the Epstein profiler rather than the popular Chapman profiler. Typical conditions of substantially low values of TEC occur during the recovery phase of the geomagnetic storm when the ionosphere is depleted. Also, the observed regular increases in slab thickness during the first few nights following the storm onset, combined with the relatively low values of TEC and N_mF_2, suggest very steep topside profiles that are difficult to accurately model with the analytical profilers alone without considering additional profile parameters (such as the upper transition level) as done in LIEDR.

Acknowledgements

This work is funded by the Royal Meteorological Institute (RMI) via the Belgian Solar-Terrestrial Centre of Excellence (STCE). The topside sounder data are provided by NASA/GSFC's Space Physics Data Facility (SPDF) and the solar/geomagnetic activity indices are from the US National Oceanic and Atmospheric Administration (NOAA).

Appendix A

Analytical ionospheric profilers

The electron density (N_e), at a given altitude h in the topside ionosphere, is considered as a sum of the constituent major ions (O^+ and H^+) densities, N_{O+} and N_{H+}, i.e.

$$N_e(h) = N_{O+}(h) + N_{H+}(h) \tag{2}$$

Each ion density profile is permitted to take one of several forms, as follows:

$$\text{(Exponential):}\quad N_i(h) = N_i(h_m)\exp\left\{-\frac{h-h_m}{H_i}\right\} \tag{3}$$

$$\text{(Chapman):}\quad N_i(h) = N_i(h_m)\exp\left\{c\left[1-\frac{h-h_m}{H_i}-\exp\left(-\frac{h-h_m}{H_i}\right)\right]\right\},\quad c=\begin{cases}0.5\,,\ \alpha-Chapman\\ 1.0\,,\ \beta-Chapman\end{cases} \tag{4}$$

$$\text{(Epstein, sech}-\text{squared):}\quad N_i(h) = N_i(h_m)sech^2\left(\frac{h-h_m}{2H_i}\right) \tag{5}$$

where N_i and H_i are the corresponding ion's (O^+ or H^+) density and scale height, and h_m is the maximum ion density height which, for both ions, is assumed to be at the height of the electron density peak, h_mF_2.

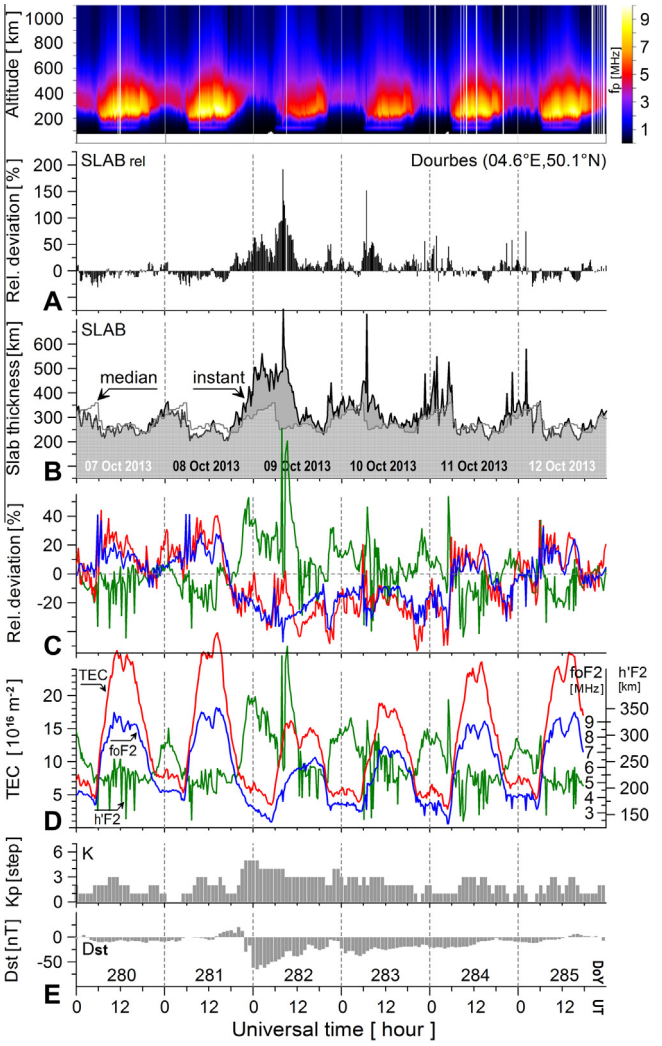

Fig. B1. LIEDR profilogram, ionospheric and magnetic activity measurements at Dourbes, 7–12 October 2013. Top panel: LIEDR real-time profilogram – ionospheric electron density profiles (as plasma frequency), constructed via LIEDR based on measurements, panels (A)-(E); (A): Relative deviation (in percentage,%) of the instantaneous ionospheric slab thickness from trailing 27-day hourly medians; (B): Instantaneous (black line) and median (grey line) slab thickness; (C): Relative deviations of TEC (red), f_oF_2 (blue), and $h'F_2$ (green); (D): Instantaneous measurements of TEC (red), f_oF_2 (blue), and $h'F_2$ (green); (E): Local magnetic K index (top) and geomagnetic storm-time index Dst (bottom). (For interpretation of the references to colour in this figure legend, the reader is referred to the web version of this article.)

Appendix B

Local ionospheric specification in real time

An operational system for deducing and imaging the vertical distribution of the electron density in the local ionosphere (LIEDR) has been recently developed (Stankov et al., 2011). At a given location, the vertical electron density profile (EDP) is deduced from local ground-based measurements of the total electron content (TEC), ionospheric vertical incidence soundings, and empirically-obtained values of the upper O^+-H^+ ion transition level (UTL). The retrieval of the corresponding vertical electron density distribution is performed in two main stages: con struction of the bottom-side electron profile (below the F_2-layer height, h_mF_2) and construction of the top-side profiles (above h_mF_2). The top-side profile is permitted to take one of several forms: Exponential, Chapman, or Epstein (cf. Appendix A). The system acquires and promptly processes the incoming measurements, computes the full-height ionospheric electron density profile, and displays the results in the form of a "profilogram". The ionospheric density profilogram is a plot of one or (usually) several vertical electron density profiles ordered sequentially over a certain period of time. Thus, the resulting 3D plot provides the colour-coded level of density (or alternatively, plasma frequency) in an altitude-time frame.

In order to demonstrate the LIEDR capabilities for detailed real-time ionospheric monitoring and imaging, a representative example is given in Fig. B1. The figure shows 6-day (07–12 Oct 2013) plots including: geomagnetic activity indices (*Dst* and local *K*), ionosonde measurements ($f_oF_2, h'F_2$) and GNSS TEC, their corresponding relative deviations from 27-day trailing medians, the ionospheric slab thickness (instantaneous, median and relative values), and, on the top, the constructed ionospheric density profilogram in the altitude range 80–1100 km. The time resolution is 15 min, except for the magnetic indices calculated once in 60 min. Thus, the combined figure provides an instant overview of the geomagnetic and ionospheric conditions at a given location.

The LIEDR system is useful for monitoring the local ionospheric dynamics even in periods of geomagnetic/ionospheric disturbances, in real time. For example, included here is a storm period of moderate intensity (with *Dst* min = −65 nT and *K* max = 5). The storm started on 8 October with a positive phase in both TEC and foF2 followed quickly by a negative phasem lasting about 72 h until 11 October. At the same time, the slab thickness experienced a sustained increase, throughout the storm, but especially during the main phase and the early hours of the recovery phase, when the relative deviations exceeded the 100% mark. The storm progression is clearly visible on the profilogram: from the bright yellow colours of the first day of the storm indicating larger plasma frequency/density, through the mostly red colour of the next day indicating a seriously depleted ionosphere of relatively low densities (plasma frequency maximum around 6 MHz), to the slowly return to the median density values on a quiet day (12 October).

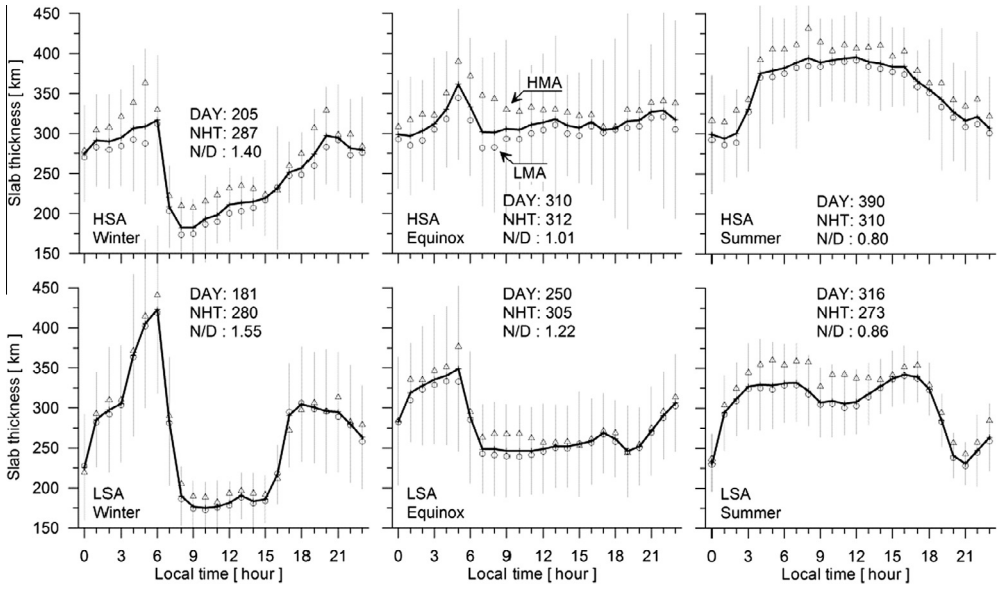

Fig. C1. Diurnal variations of the slab thickness during low (bottom panels) and high (top panels) solar activity, as deduced from measurements at Dourbes (50.1° N, 04.6° E). Solid lines show the average variations based on data from all geomagnetic conditions, the 'Δ'symbols denote the average values observed during high magnetic activity (HMA, $K_p \geqslant 3$) and the 'o' symbols denote the values during low magnetic activity (LMA, $K_p < 3$) conditions. The standard deviations (2σ) denoted with vertical bars.

Appendix C

Ionospheric slab thickness—definition and variability

The ionospheric slab thickness (τ) is defined (Davies, 1990) as the ratio of the Total Electron Content (TEC) to the maximum ionospheric F_2-layer electron density (N_mF_2), or in terms of the F_2 critical frequency (foF2), $\tau = TEC/(1.24 \times 10^{-6}(foF2)^2)$, where TEC is measured in TEC units (1 TECU $= 10^{16}$ electrons per square metre), foF2 in MHz, and τ in metres. In other words, τ represents the equivalent slab thickness/depth of an idealised ionosphere which has the same electron content as the actual ionosphere but uniform electron density equal to the maximum electron density.

The mean diurnal variations of the slab thickness observed at Dourbes (Fig. C1) (Stankov and Warnant, 2009) are characterised with night-time values that are substantially higher than the day-time values during winter (night-to-day ratio between 1.40 at high solar activity (HSA) and 1.55 at low solar activity (LSA), but higher day-time and lower night-time values during summer (night-to-day ratio of 0.80 HSA to 0.86 LSA). A pre-dawn increase of the slab thickness is observed in the winter and equinox seasons, most pronounced during LSA winter between 05:00 LT and 06:00 LT, when average values exceed 400 km.

The high solar activity induces higher slab thickness values, both during night (up to 14%) and day (up to 24%). Most prominent are the seasonal changes. During LSA, the average day-time values increase from 181 km in winter to 316 km in summer, while during HSA, the values almost double from winter (205 km) to summer (390 km). The night time values however, do not experience such large variability from winter to summer. There is comparatively small diurnal variation in τ during the equinoctial months.

References

Banks, P.M., Kockarts, G., 1973. Aeronomy. Academic Press, New York and London.

Benson, R.F., 2010. Four decades of space-borne radio sounding. Radio Sci. Bull. 333, 24–44.

Bent, R.B., Llewellyn, S.K., Schmid, P.E. Description and evaluation of the Bent ionospheric model, vols. 1, 2, and 3, Space and Missile Systems Organization Report SAMSO TR-72-239, National Technical Information Service, AD-753-081, -082, -083, Springfield, VA, 1972.

Bilitza, D., Reinisch, B., Benson, R., Grebowsky, J., Papitashvili, N., Huang, X., Schar, W., Hills, K., 2003. Online data base of satellite sounder and in-situ measurements covering two solar cycles. Adv. Space Res. 31 (3), 769–774.

Bilitza, D., Huang, X., Reinisch, B., Benson, R., Hills, H.K., Schar, W.B., 2004 (Topside ionogram scaler with true height algorithm (TOPIST): automated processing of ISIS topside ionograms). Radio Sci. 39 (1), RS1S27. http://dx.doi.org/10.1029/2002RS002840.

Bilitza, D., 2004. A correction for the IRI topside electron density model based on Alouette/ISIS topside sounder data. Adv. Space Res. 33 (6), 838–843.

Booker, H.C., 1977. Fitting of multi-region ionospheric profiles of electron density by a single analytical function of height. J. Atmos. Terr. Phys. 39 (1), 619–623.

Buonsanto, M.J., 1999. Ionospheric storms – a review. Space Sci. Rev. 88, 563–601.

Davies, K., 1990. Ionospheric Radio. Peter Peregrinus Ltd., London, UK.

Feltens, J., 2007. Development of a new three-dimensional mathematical ionosphere model at European Space Agency/European Space Operations Centre. Space Weather 5, S12002.

Fonda, C., Coïsson, P., Nava, B., Radicella, S.M., 2005. Comparison of analytical functions used to describe topside electron density profiles with satellite data. Ann. Geophys. 48 (3), 491–495.

Fuller-Rowell, T.J., Codrescu, M.V., Moffett, R.J., Quegan, S., 1994. Response of the thermosphere and ionosphere to geomagnetic storms. J. Geophys. Res. 99 (A3), 3893–3914.

Hernandez-Pajares, M., Juan, J.M., Sanz, J., Orus, R., Garcia-Rigo, A., Feltens, J., Komjathy, A., Schaer, S.C., Krankowski, A., 2009. The IGS VTEC maps: a reliable source of ionospheric information since 1998. J. Geod. 83 (3), 263–275.

Jackson, J.E., Warren, E.S., 1969. Objectives, history, and principal achievements of the topside sounder and ISIS programs. Proc. IEEE 57, 861–865.

Jackson, J.E., 1969 (The reduction of topside ionograms to electron-density profiles). Proc. IEEE, 960–976.

Jackson, J.E., Schmerling, E.R., Whitteker, J.H., 1980. Mini-review on topside sounding. IEEE Trans. Antennas Propag. AP-28, 184–288.

Jackson, J.E., 1988. Results from Alouette 1, Explorer 20, Alouette 2 and Explorer 31, NSSDC Report 88–10. National Space Science Data Center, Greenbelt, MD.

Kutiev, I., Muhtarov, P., 2001 (Modeling of midlatitude F region response to geomagnetic activity). J. Geophys. Res. 106 (A-8), 15501–15509. http://dx.doi.org/10.1016/S0273-1177(98)00114-8.

Kutiev, I., Watanabe, S., Otsuka, Y., Saito, A., 2005. Total electron content behavior over Japan during geomagnetic storms. J. Geophys. Res. 110, A01308.

Kutiev, I., Marinov, P.G., Watanabe, S., 2006a. Model of topside ionosphere scale height based on topside sounder data. Adv. Space Res. 37 (5), 943–950.

Kutiev, I., Otsuka, Y., Saito, A., Watanabe, S., 2006b. GPS observations of post-storm TEC enhancements at low latitudes. Earth Planets Space 58 (11), 1479–1486.

Nsumei, P., Reinisch, B.W., Huang, X., Bilitza, D., 2012 (New Vary-Chap profile of the topside ionosphere electron density distribution for use with the IRI model and the GIRO real time data). Radio Sci. 47, RS0L16.

Ondoh, T., 1967. Morphology of disturbed topside ionosphere for 1962–1964. J. Radio Res. Lab. 14, 267–279.

Proelss, G.W., 1984. Local time dependence of magnetic storm effects on the atmosphere at middle latitudes. Ann. Geophys. 2, 481–485.

Reinisch, B.W., Huang, X., 2001. Deducing topside profiles and total electron content from bottomside ionograms. Adv. Space Res. 27 (1), 23–30.

Reinisch, B.W., Nsumei, P., Huang, X., Bilitza, D.K., 2007. Modeling the F2 topside and plasmasphere for IRI using IMAGE/RPI and ISIS data. Adv. Space Res. 39 (5), 731–738.

Reinisch, B.W., Galkin, I.A., Khmyrov, G.M., et al., 2009. New Digisonde for research and monitoring applications. Radio Sci. 44 (1), RS0A24.

Sato, T., 1968. Electron concentration variations in the topside ionosphere between 60 N and 60 S geomagnetic latitude associated with geomagnetic disturbances. J. Geophys. Res. 73 (1), 6225–6241.

Stankov, S.M., Warnant, R., 2009. Ionospheric slab thickness – analysis, modelling and monitoring. Adv. Space Res. 44 (11), 1295–1303.

Stankov, S.M., Stegen, K., Warnant, R., 2010. Seasonal variations of storm-time TEC at European middle latitudes. Adv. Space Res. 46 (10), 1318–1325.

Stankov, S.M., Stegen, K., Muhtarov, P., Warnant, R., 2011. Local ionospheric electron density profile reconstruction in real time from simultaneous ground-based GNSS and ionosonde measurements. Adv. Space Res. 47 (7), 1172–1180.

Stankov, S.M., Jodogne, J.C., Kutiev, I., Stegen, K., Warnant, R., 2012. Evaluation of automatic ionogram scaling for use in real-time ionospheric density profile specification: Dourbes DGS-256/ART-IST-4 performance. Ann. Geophys. 55 (2), 283–291.

Tulasi Ram, S., Su, S.Y., Liu, C.H., Reinisch, B., McKinnel, L.A., 2009 (Topside ionospheric effective scale heights (HT) derived with ROC-SAT-1 and ground-based ionosonde observations at equatorial and midlatitude stations). J. Geophys. Res. 114, A10309.

Verhulst, T., Stankov, S.M., 2013. The topside sounder database – Data screening and systematic biases. Adv. Space Res. 51 (11), 2010–2017.

Verhulst, T., Stankov, S.M., 2014. Evaluation of ionospheric profilers using topside sounding data. Radio Science 49 (3), 181–195. http://dx.doi.org/10.1002/2013RS005263.

Warren, E.S., 1969. The topside ionosphere during geomagnetic storms. Proc. IEEE 57, 1029–1036.